



HAL
open science

Layered Vanadium Phosphates as Electrodes for Electrochemical Capacitors Part II: The Case of VOPO₄ •CTAB and K_{0.5} VOPO₄ •1.5H₂O

Jorge Alexis Zúñiga Martínez, Sara Elena González Náñez, Etienne Le Calvez, Raúl Lucio Porto, Iván Eleazar Moreno Cortez, Thierry Brousse, Luis Alberto López Pavón

► To cite this version:

Jorge Alexis Zúñiga Martínez, Sara Elena González Náñez, Etienne Le Calvez, Raúl Lucio Porto, Iván Eleazar Moreno Cortez, et al.. Layered Vanadium Phosphates as Electrodes for Electrochemical Capacitors Part II: The Case of VOPO₄ •CTAB and K_{0.5} VOPO₄ •1.5H₂O. Journal of The Electrochemical Society, 2021, 168 (9), pp.090520. 10.1149/1945-7111/ac23a0 . hal-03355965

HAL Id: hal-03355965

<https://hal.science/hal-03355965>

Submitted on 17 Nov 2021

HAL is a multi-disciplinary open access archive for the deposit and dissemination of scientific research documents, whether they are published or not. The documents may come from teaching and research institutions in France or abroad, or from public or private research centers.

L'archive ouverte pluridisciplinaire **HAL**, est destinée au dépôt et à la diffusion de documents scientifiques de niveau recherche, publiés ou non, émanant des établissements d'enseignement et de recherche français ou étrangers, des laboratoires publics ou privés.

Layered Vanadium Phosphates as Electrodes for Electrochemical Capacitors
Part II: The Case of $\text{VOPO}_4 \cdot \text{CTAB}$ and $\text{K}_{0.5}\text{VOPO}_4 \cdot 1.5\text{H}_2\text{O}$

Jorge Alexis Zúñiga Martínez^{a,b}, Sara Elena González Náñez^{a,b}, Etienne Le Calvez^{c,d}, Raúl Lucio Porto^{a,b,*}, Iván Eleazar Moreno Cortez^{a,b}, Thierry Brousse^{c,d}, Luis Alberto López Pavón^{a,b}

^a Universidad Autónoma de Nuevo León, Facultad de Ingeniería Mecánica y Eléctrica, San Nicolás de los Garza, 66455, Nuevo León, México

^b Universidad Autónoma de Nuevo León, Centro de Innovación, Investigación y Desarrollo en Ingeniería y Tecnología, Apodaca, 66600, Nuevo León, México

^c Université de Nantes, CNRS, Institut des Matériaux Jean Rouxel, IMN, F-44000 Nantes, France

^d Réseau sur le Stockage Electrochimique de l'Energie, CNRS FR 3459, 80039 Amiens Cedex, France

*corresponding author, e-mail: raul.lucioprt@uanl.edu.mx

Phone: +52 (81) 1340-4000 ext 1504

Keywords: Vanadium Phosphate, Electrochemical Capacitor, Supercapacitor, Ion Intercalation

Abstract

In the present work two layered vanadium phosphates were prepared, $\text{VOPO}_4 \cdot \text{CTAB}$ and $\text{K}_{0.5}\text{VOPO}_4 \cdot 1.5\text{H}_2\text{O}$ as electrode materials for electrochemical capacitors. These materials contain different molecular species in their interlayer space leading to an electrochemical behavior that drastically differs from the crystalline phase $\text{VOPO}_4 \cdot 2\text{H}_2\text{O}$, with water molecules in the interlayer space. In the case of $\text{VOPO}_4 \cdot \text{CTAB}$, it was found that CTAB molecules block the pathway of electrolyte ions into the crystalline structure avoiding an intercalation/deintercalation process. In the case of $\text{K}_{0.5}\text{VOPO}_4 \cdot 1.5\text{H}_2\text{O}$, the K^+ ions from the crystalline structure hinder the intercalation/deintercalation process leading around 73 and 71 percent of the charge arise from a capacitive process in 3M LiOH and 3M KOH, respectively.

1. Introduction

Electrochemical Capacitors (ECs) so-called supercapacitors, are energy storage devices which can exhibit two charge storage processes. The first one is the capacitive process

related to the accumulation of charges by electrostatic forces in the electrode-electrolyte interface through the electrical double layer (EDL) formation. This process is the predominant one for carbon-based ECs. The second one is pseudocapacitance which consists in storing charges due to the fast and reversible surface redox reactions, giving rise to a capacitive-like behavior, i.e. a linear increase of stored charge while the voltage window is expanded [1-3]. Additionally, some electrode materials used in ECs exhibit an intercalation/deintercalation process during charge and discharge which gives rise to redox waves superimposed to capacitive/pseudocapacitive electrochemical response. This process is typically found in battery-type electrode materials [4-8] and it takes place in the 1, 2 or 3D tunnels of their crystalline structure. Recently, the intercalation/deintercalation process has been reported by our group in different metal phosphates such as $\text{MnPO}_4 \cdot \text{H}_2\text{O}$ and $\text{VOPO}_4 \cdot 2\text{H}_2\text{O}$ [9,10] with 1D and 2D tunnels respectively, which have been proposed as electrode materials for ECs. The same behavior has also been reported, coupling ions intercalation and capacitive/pseudocapacitive features, such as layered birnessite (MnO_2), V_2O_5 , TiO_2 , Nb_2O_5 , and MoO_2 [11-24].

The previous reports [9,10] on our metal phosphates show the coexistence of the intercalation/deintercalation process (Faradaic behavior) with the capacitive and pseudocapacitive processes. In the case of $\text{VOPO}_4 \cdot 2\text{H}_2\text{O}$, it was shown for the first time that the intercalation/deintercalation process is present even at high rates of charge/discharge. It is worth to highlight that in both metal phosphates, the tunnels in their crystalline structure contain water molecules. It has been argued in several reports that water molecules allow ion mobility through crystalline inorganic materials [25-27] enabling the intercalation/deintercalation process. Hence, it was also supposed that the origin of the intercalation/deintercalation process in $\text{VOPO}_4 \cdot 2\text{H}_2\text{O}$ was caused by the presence of water molecules.

In order to validate the above assumption, we prepared two layered vanadium phosphates with different chemical species within the interlayer spaces, like CTAB molecules or K^+ ions. The aim is to determine if the intercalation/deintercalation process is possible, or if CTAB molecules hinder the intercalation of electrolyte cations in the 2D tunnels by a blocking mechanism. In the case of K^+ ions that are part of the crystalline structure, it is not quite clear

if they can be part of the charge-discharge process or if they remain as structural cations of the layered material.

2. Methodology

Synthesis of VOPO₄•CTAB

An appropriate amount of hexadecyltrimethylammonium bromide (CTAB, Sigma-Aldrich 98%) was dissolved in deionized water to obtain a concentration of 5 wt %. Then, K₂HPO₄ (Sigma-Aldrich, 97%) was added to the above mixture to obtain a molar ratio CTAB/ K₂HPO₄ of 1. The temperature of the solution was increased to 70°C and kept at this temperature for one hour. A solution of VOSO₄ (Sigma-Aldrich, 98%) was added dropwise to keep a molar ratio VOSO₄/ K₂HPO₄ of 0.8. After 24 hours of reaction, the yellow powder was recovered by filtration and washed several times with water and acetone. Finally, the precipitate was dried at room temperature.

Synthesis of Nanostructured K_{0.5}VOPO₄•1.5H₂O

An appropriate amount of CTAB was dissolved in deionized water to obtain a concentration of 5 wt %. Then, K₂HPO₄ (Sigma-Aldrich, 97%) was added to the above mixture to obtain a molar ratio CTAB/ K₂HPO₄ of 1. The temperature of the solution was increased to 70°C and kept at this temperature for one hour. A solution of VOSO₄ (Sigma-Aldrich, 98%) was added dropwise to keep a molar ratio VOSO₄/ K₂HPO₄ of 1.2. After 24 hours of reaction, a green powder was recovered by filtration and washed several times with water and acetone. Finally, the precipitate was dried at room temperature.

Synthesis of VOPO₄•2H₂O

Following the sonication method proposed by Park et. al. [28], an appropriate amount of V₂O₅, (Fermont, 98%), H₃PO₄ (CTR, 85%) and deionized water H₂O were mixed to obtain a solution with a fixed molar ratio of V₂O₅: H₃PO₄:H₂O = 1 : 50 : 604. The solution was sonicated at 37 kHz during 45 min (Fisherbrand, FB11201, power 120 W). Then the yellow powder was recovered by filtration and washed several times with water and acetone. Finally, the precipitate was dried at room temperature.

2.1 Material Characterization

The X-ray diffraction pattern (XRD) was collected with an Empyrean PANalytical X'Pert Pro diffractometer with an X'Celerator detector and CuK_α radiation ($\lambda = 1.5406 \text{ \AA}$) operated at 45 kV and 40 mA. The scans were performed in the 2θ range from 5 to 90° with a step scan of 0.02° and 1s per step in a continuous mode. The morphology of the vanadium phosphates was analyzed by scanning electron microscopy (SEM), using FEI Nova NanoSEM with a Field Emission Gun and by transmission electron microscopy (TEM), Hitachi H9000-NAR. FTIR analyses were performed with a Thermo Scientific model Nicolet 6700 spectrophotometer. Pellets were prepared with KBr in a weight ratio of 1:50 (sample:KBr). The spectra were collected with a resolution of 4 cm^{-1} and averaged over 32 scans. The BET surface areas were measured using an Autosorb II BET apparatus.

2.2 Electrochemical Characterization

The electrodes were prepared from a mixture of active material, carbon black and polytetrafluoroethylene (PTFE, Sigma-Aldrich) in a mass ratio = 70:20:10 respectively. The electrode components were mixed with acetone. The resulting paste was cold rolled into a $100 \text{ }\mu\text{m}$ thick film and pressed between two stainless steel grids at 1 GPa. The active material mass loading was 7 mg.cm^{-2} . A Three-electrode cell was used with a platinum grid as the counter-electrode and an appropriate reference electrode was used, depending on the pH of the electrolyte (Ag/AgCl for neutral pH or Hg/HgO for more basic pH).

The electrochemical measurements were performed using an SP-150 potentiostat-galvanostat (Biologic Instruments). The electrochemical behavior of the electrode material was studied by cyclic voltammetry, chronopotentiometry and electrochemical impedance spectroscopy (EIS). For the EIS tests, an amplitude of 10 mV was used with a frequency range from 10 mHz to 100 kHz. The specific capacitance $C \text{ (Fg}^{-1}\text{)}$ was obtained from Equation 1. Where Q is the charge in C, obtained from the integration of the area of the cyclic voltammogram either in oxidation or reduction, ΔV is the width of the electrochemical window in V and m is the mass of active material in grams.

$$C \text{ (Fg}^{-1}\text{)} = Q(\Delta Vm)^{-1} \quad (1)$$

3. Results

3.1 Material synthesis and characterization

The synthesis and the description of $\text{VOPO}_4 \cdot 2\text{H}_2\text{O}$ can be found in our previous report [10]. The XRD pattern is included in Figure 1a. There are water molecules between the layers of VOPO_4 units with an interlayer distance of 7.40 Å. The synthesis of $\text{VOPO}_4 \cdot \text{CTAB}$ using the precipitation method proceeds in two steps. First, there is a precipitation achieved by the VOSO_4 and KH_2PO_4 precursors. Initially, the color of the solution is blue, and during the reaction time turns out to yellow by oxidation caused by the combination of oxygen dissolved in the solution, the reaction temperature and reaction time. In this way, the vanadium ions with a formal charge of 4^+ in VOSO_4 leads to a yellow compound indicating a change in the oxidation state of vanadium cations to V^{5+} . Figure 1a shows the resulting XRD pattern with broad (hkl) peaks indicative of a nanostructured material. This material can also be indexed to the PDF #36-1472 card with tetragonal structure and space group P4/nmm as it is the case for $\text{VOPO}_4 \cdot 2\text{H}_2\text{O}$. However, there is a shift of the (001) reflection to the lower 2θ indicating an increase in the interlayer distance from 7.40 Å to 10.03 Å [29] originated by the incorporation of CTAB molecules into the crystalline structure, thus replacing the water molecules.

Modifying the molar ratio of $\text{VOSO}_4/\text{K}_2\text{HPO}_4$ in the presence of CTAB, leads to a green powder. The XRD pattern of Figure 1a shows well defined peaks that can be indexed to $\text{K}_{0.5}\text{VOPO}_4 \cdot 1.5\text{H}_2\text{O}$ (01-081-1930 card), with a Triclinic crystal system and a P-1 space group. This is also a layered material as in the case of $\text{VOPO}_4 \cdot 2\text{H}_2\text{O}$. However, there are important differences as a consequence of the incorporation of K^+ ions into the crystalline structure. First, there is a reduction of the interlayer spacing down to 6.38 Å. This is originated by the negatively charged layers that are attracted closer due to the presence of K^+ ions by electrostatic interactions [30]. According to Wang et al., there is a partial reduction of V^{5+} cations to V^{4+} , suggesting a mixed valence for vanadium cations. The layers of bound vanadium and phosphorus polyhedra are displaced with respect to each other to form large cavities where K^+ cations and H_2O molecules are located. The other water molecules remain bound to vanadium atoms. Thus, the K^+ cations run parallel to the a axis and alternate with water molecules in the b axis.

In summary, layered vanadium phosphates were prepared with different species in the interlayer space. Figure SI1, 1a, 1b and 1c show the crystalline structure of the $\text{VOPO}_4 \cdot 2\text{H}_2\text{O}$ (as the reference compound), $\text{VOPO}_4 \cdot \text{CTAB}$ and $\text{K}_{0.5}\text{VOPO}_4 \cdot 1.5\text{H}_2\text{O}$. The electrochemical

behavior of these three compounds will allow to determine the influence of structural parameters on the charge storage processes.

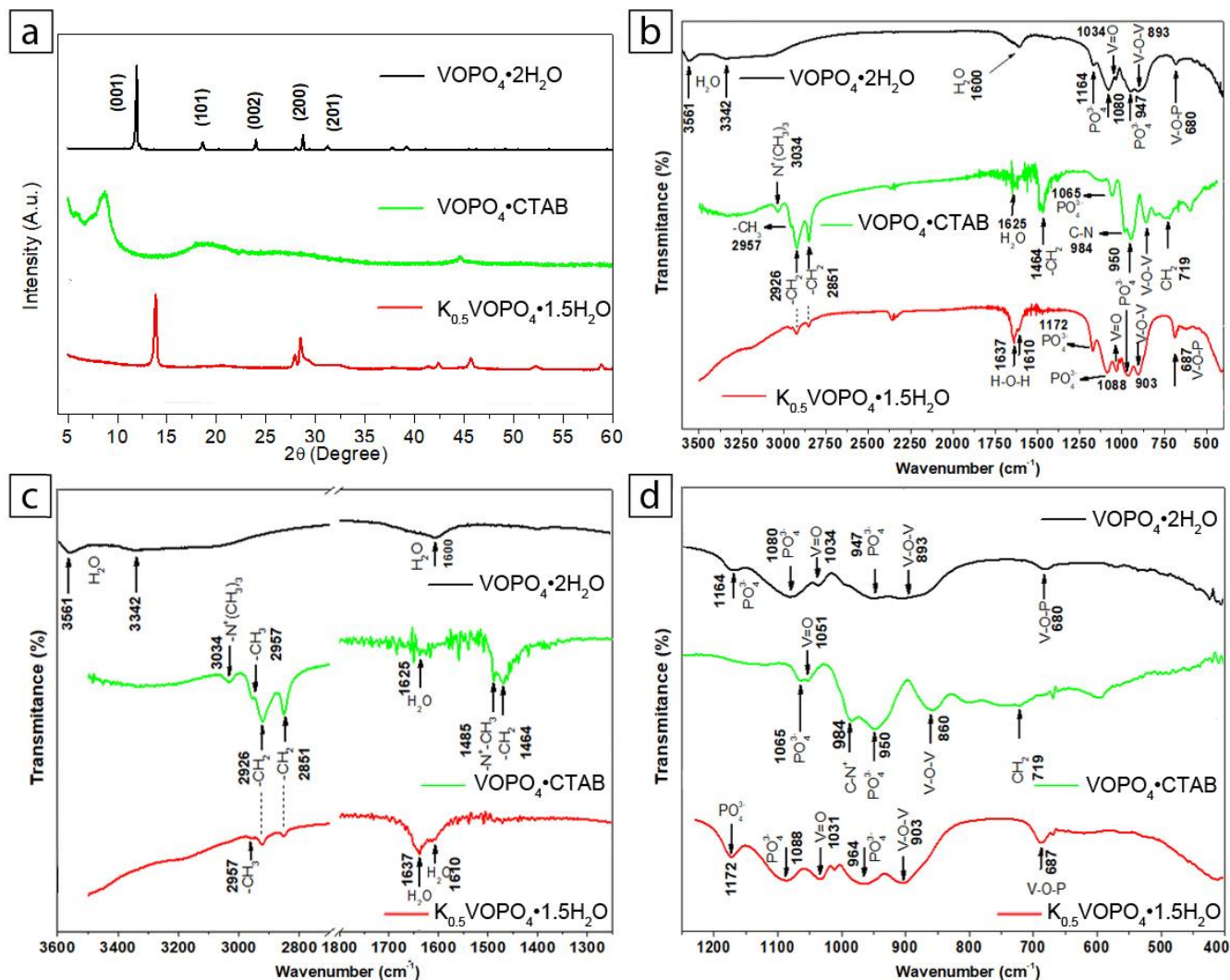


Figure 1. a) XRD patterns of the 3 different layered vanadium phosphates, b) FTIR spectra of vanadium phosphates c) and d) Magnification of FTIR spectra.

Figure 1b shows the FTIR spectroscopy confirming the presence of several functional groups of vanadium phosphates that include the stretching vibrations of V-O-P, V=O and P-O₄. For clarification, Figure 1c and 1d shows a magnification of Figure 1b. The spectrum of $\text{VOPO}_4 \cdot 2\text{H}_2\text{O}$ was already discussed in our previous report [10] confirming the formation of vanadium phosphates with water molecules in the interlayer space as evidenced by the bands at 3342 and 3561 cm^{-1} [10].

However, a different spectrum was obtained for $\text{VOPO}_4 \cdot \text{CTAB}$. First, the presence of CTA^+ cation (from CTAB molecule) is evidenced by the band at 2957 cm^{-1} that is attributed to the asymmetric stretching vibrations mode of CH_3 groups [31,32]. The band at 2926 and 2851 cm^{-1} corresponds to the asymmetric and symmetric stretching vibrations of CH_2 groups, respectively [31-35,39]. Additionally, the bands centered at 1464 and 719 cm^{-1} are ascribed to the scissoring and rocking mode of the CH_2 group, respectively. These bands are associated to a certain degree of order of the intercalated CTA^+ ion in layered inorganic materials [31-34]. Second, the characteristic bands of the head group of CTA^+ cation in the spectra, also indicate a certain degree of order of the surfactant chains in the interlayer space of inorganic materials [31,34,35]. The bands at 3034 , 1485 and 984 cm^{-1} correspond to the asymmetric stretching of $\text{N}^+(\text{CH}_3)_3$, the bending mode of N^+-CH_3 and to $\text{C}-\text{N}^+$ respectively [31-33,35-37]. Third, the bands of $\text{V}-\text{O}-\text{V}$ and $\text{V}^{5+}=\text{O}$ present a blue shift to 860 and 1051 cm^{-1} respectively [30,39]. This may be originated by the presence of intercalated CTA^+ cation that changes their frequency of vibration. Additionally, the bands that correspond to PO_4 groups are centered at 950 and 1065 cm^{-1} . Fourth, the bands at 3342 and 3561 cm^{-1} associated to water molecules bonded by hydrogen bonds to PO_4 groups [40] disappear indicating that there are no water molecules in the interlayer space as in the case of $\text{VOPO}_4 \cdot 2\text{H}_2\text{O}$, only a weak band at 1625 cm^{-1} that correspond to $\text{H}-\text{O}-\text{H}$ [41]. This suggests that the CTA^+ cations are intercalated and replace the water molecules in the interlayer space of $\text{VOPO}_4 \cdot \text{CTAB}$. This agrees with the XRD results.

In the case of $\text{K}_{0.5}\text{VOPO}_4 \cdot 1.5\text{H}_2\text{O}$ the bands at 2957 , 2926 and 2851 cm^{-1} are assigned to asymmetric stretching of CH_3 [31-32] and asymmetric and symmetric stretching vibrations of CH_2 groups, respectively [31-35,39]. These weak bands indicate the presence of the CTAB molecules in a lower concentration than in the previous case. However, the bands that correspond to the head group ($\text{N}^+(\text{CH}_3)_3$, N^+-CH_3 and $\text{C}-\text{N}^+$) of CTA^+ cation, and the bands assigned to the scissoring and rocking mode of the CH_2 group are not present. This indicates that CTAB molecules are not intercalated in the interlayer space, in agreement with XRD data. Thus, it is suggested that CTAB molecules are only adsorbed at the surface of these particles. Furthermore, the bands centered at 687 , 903 and 1031 cm^{-1} correspond to the bending vibration of $\text{V}-\text{O}-\text{P}$, the stretching vibration of $\text{V}-\text{O}-\text{V}$ and the stretching vibration of $\text{V}^{5+}=\text{O}$, respectively [38,40,41]. The bands of the PO_4^{3-} group are centered at 964 and 1088 cm^{-1} and both can be assigned to asymmetric stretching vibration. The band at 1172 cm^{-1} also belongs

to the stretching vibration of the PO_4^{3-} group [40]. The bands at 1637 and 1610 cm^{-1} are ascribed to the stretching vibration of H-O-H in the crystalline structure [41].

Figure SI2 shows the SEM and TEM images of the electrode materials. In all the cases the morphology of the nanoparticles consists in platelets with a size of 230 nm and 1 μm and the thickness is 20 and 40 nm for $\text{VOPO}_4\cdot\text{CTAB}$ and $\text{K}_{0.5}\text{VOPO}_4\cdot 1.5\text{H}_2\text{O}$, respectively. The absorption-desorption isotherms are shown in Figure SI3. The BET surface areas are 14, 2 and 11 m^2g^{-1} for $\text{VOPO}_4\cdot 2\text{H}_2\text{O}$, $\text{VOPO}_4\cdot\text{CTAB}$ and $\text{K}_{0.5}\text{VOPO}_4\cdot 1.5\text{H}_2\text{O}$, respectively. No hysteresis was observed in the isotherms for the later cases, indicating the lack of mesopores.

3.2 Electrochemical characterization

It was demonstrated in part 1 of this work [10] that in 3M LiOH, Li^+ cation intercalates into the 2D tunnels of $\text{VOPO}_4\cdot 2\text{H}_2\text{O}$ that are generated by the layers of VO_6 and PO_4 groups with an interlayer distance of 7.40 Å [42-44]. Water molecules are located between the layers. According to the coupling of Trassati and Dunn methods used in our previous work to deconvolute the charge storage mechanisms from cyclic voltammograms, the cation intercalation takes place across the whole potential window, and it is still significant even at scan rates as high as 100 mVs^{-1} . At low scan rates (5 mVs^{-1}) the intercalation process contributes to 80 % of the accumulated charge. Moreover, 19 % of the charge comes from pseudocapacitive charge process and only 1 percent from double layer capacitance (EDL). At high scan rate (100 mVs^{-1}) Li^+ cation intercalation still contributes to 47 % of the accumulated charge.

Nevertheless, in the case of $\text{VOPO}_4\cdot\text{CTAB}$ in 3M LiOH the electrochemical signature is rectangular in the applied voltage as is shown in Figure 2a. However, the capacitive behavior is lost at scan rates above 10 mVs^{-1} as shown in Figure SI4a. Additionally, the maximum specific capacitance is low, around 10 Fg^{-1} that corresponds to 20 μFcm^{-2} , in the range of the areal capacitance (20-50 μFcm^{-2}), that arises from EDL formation [45,46]. Thus, it is reasonable to attribute the electrochemical response mainly to an EDL process. The use of 3M KOH with K^+ being larger than Li^+ (unsolvated ions) only aggravates the electrochemical response leading to the loss of the capacitive behavior at any scan rate tested in this work (see also Figure SI4b). Thus, the lack of intercalation process in this electrode material may

be related to its crystalline structure. $\text{VOPO}_4 \cdot \text{CTAB}$ also consists in layers of VO_6 and PO_4 groups as in the case of $\text{VOPO}_4 \cdot 2\text{H}_2\text{O}$. However, its interlayer distance is larger (10.03 \AA) than in the previous case (7.40 \AA) due to the presence of CTAB molecules between the layers. Hence, in this case the electrolyte cations, either Li^+ or K^+ cannot be intercalated into the crystalline structure of $\text{VOPO}_4 \cdot \text{CTAB}$ due to the presence of CTAB molecules that blocks the pathway to the 2D tunnels.

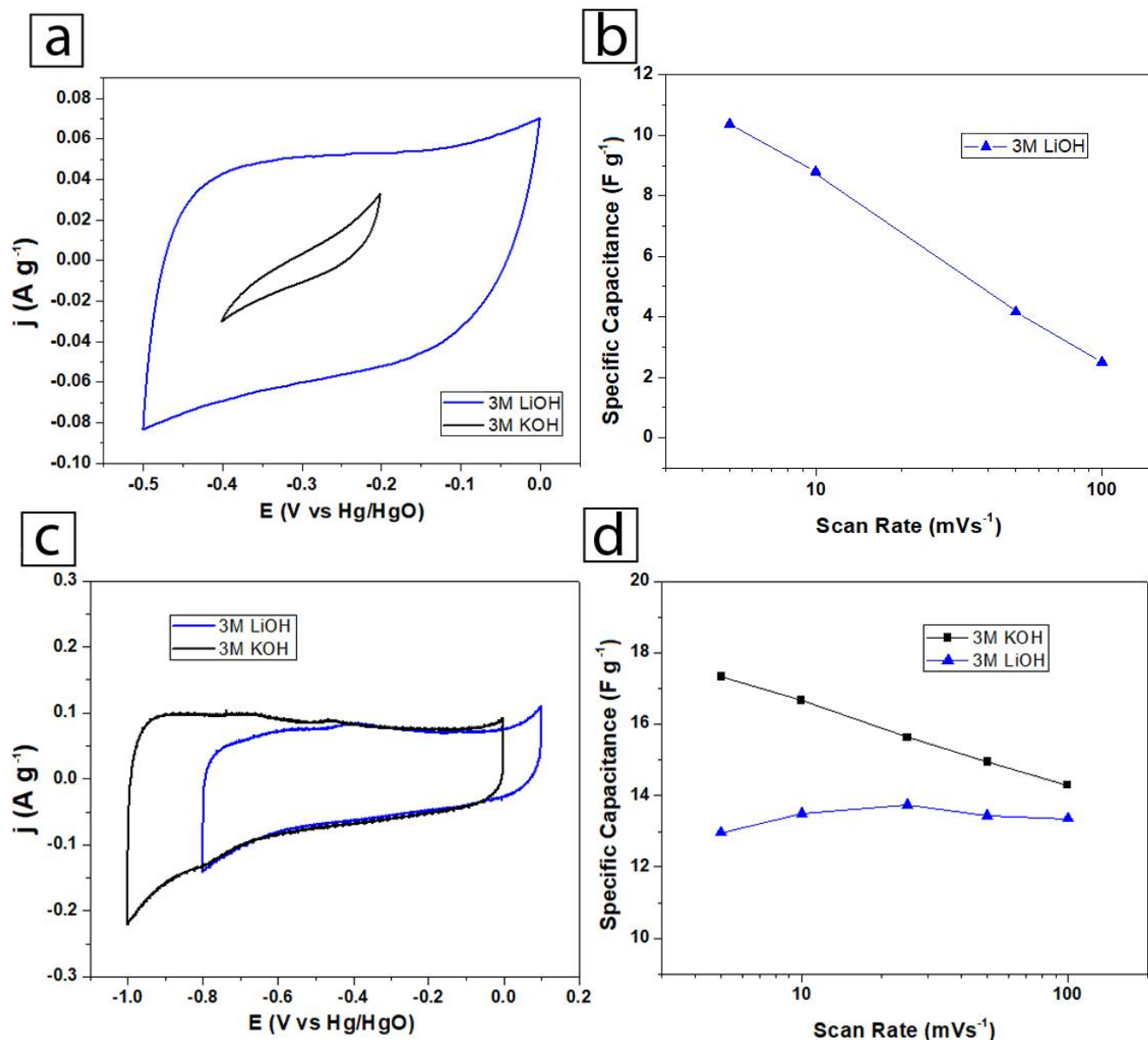


Figure 2. Electrochemical windows of $\text{VOPO}_4 \cdot \text{CTAB}$ in 3M LiOH and 3M KOH at the scan rate of 5 mVs^{-1} . b) Specific capacitance of $\text{VOPO}_4 \cdot \text{CTAB}$ in 3M LiOH as a function of the scan

rate. c) Electrochemical windows of $K_{0.5}VOPO_4 \cdot 1.5H_2O$ in 3M LiOH and 3M KOH at the scan rate of 5 mVs^{-1} . d) Specific capacitance of $K_{0.5}VOPO_4 \cdot 1.5H_2O$ in 3M LiOH and 3M KOH as a function of the scan rate.

On the other hand, Figure 2c shows a different electrochemical response for $K_{0.5}VOPO_4 \cdot 1.5H_2O$. In 3M LiOH, the voltammogram exhibits a quasi-rectangular shape, with reversible redox waves observed at -0.4 V and 0.3 V vs Hg/HgO in the cathodic and anodic sweep respectively, thus indicating the presence of a faradaic contribution. In 3M KOH, a quasi-rectangular shape is also obtained indicating a capacitive-like behavior. The voltammogram exhibits reversible redox waves observed at -0.65 V and 0.75 V vs Hg/HgO for the cathodic and anodic sweep, respectively. The evolution of cyclic voltammograms as a function of scan rate for both electrolytes are shown in Figure SI5a and SI5b. It is remarkable that as the scan rate increases the rectangular shape of the cyclic voltammograms remains quasi-rectangular up to 100 mVs^{-1} . Despite the redox waves on the voltammograms that could lead to a large stored charge, the specific capacitance is lower than for $VOPO_4 \cdot 2H_2O$ in the same electrolytes [10]. However, the areal capacitance is 118 and $159 \mu\text{Fcm}^{-2}$ in 3M LiOH and 3M KOH respectively, larger than $50 \mu\text{Fcm}^{-2}$ that can be related to pure EDL formation. This indicates that a different mechanism is involved in the charge storage process for $K_{0.5}VOPO_4 \cdot 1.5H_2O$.

In order to determine the charge storage process, the values of the b parameter, which is described elsewhere [6,10], are shown in Figure SI6 for $K_{0.5}VOPO_4 \cdot 1.5H_2O$ in 3M LiOH and 3M KOH. All b values are above 0.8 in both electrolytes in all the applied potential window, indicating a non-diffusive (intercalation) process. However, as it was discussed in the first part of this work [10], it is necessary to use the coupled Trasatti-Dunn methods [10,41,42] to determine the origin of the charge, and perform a deconvolution of the charge storage mechanisms of $K_{0.5}VOPO_4 \cdot 1.5H_2O$ in 3M LiOH and 3M KOH. This methodology allows to estimate the contribution of EDL formation, pseudocapacitance and Faradaic process to the stored charge. The methodology is described in supporting information. The results are shown in Figure 3. In both electrolytes, the capacitive (EDL and pseudocapacitance) processes contribute to the larger amount of stored charges, 73 and 71 %, respectively (see Figure 3b and 3d). However, 27 % of stored charge arises from the diffusive process (see Figure 3a) in 3M LiOH at the low scan rate of 5 mVs^{-1} . The diffusive charge is more significant

in the range -0.8 to -0.4 V vs Hg/HgO and -0.4 to 0.1 V vs Hg/HgO. In 3M KOH, the contribution of diffusive charge is 29 % at the scan rate of 5 mVs⁻¹, and the large amount of this charge process occurs from -1.0 to -0.6 V vs Hg/HgO (see Figure 3c). This indicates that in both electrolytes an ion intercalation/deintercalation process contributes to the overall charge storage process which also explains the redox waves in the cyclic voltammograms (Figure 2c). At fast scan rate (100 mVs⁻¹) the charge originating from a diffusive process is around 5 % (Figure 3b and d) in both electrolytes. From Figure 3 it is obvious that for this electrode material the amount of diffusive charge is low and practically constant at high scan rate (Figures S17) in the complete operational potential window.

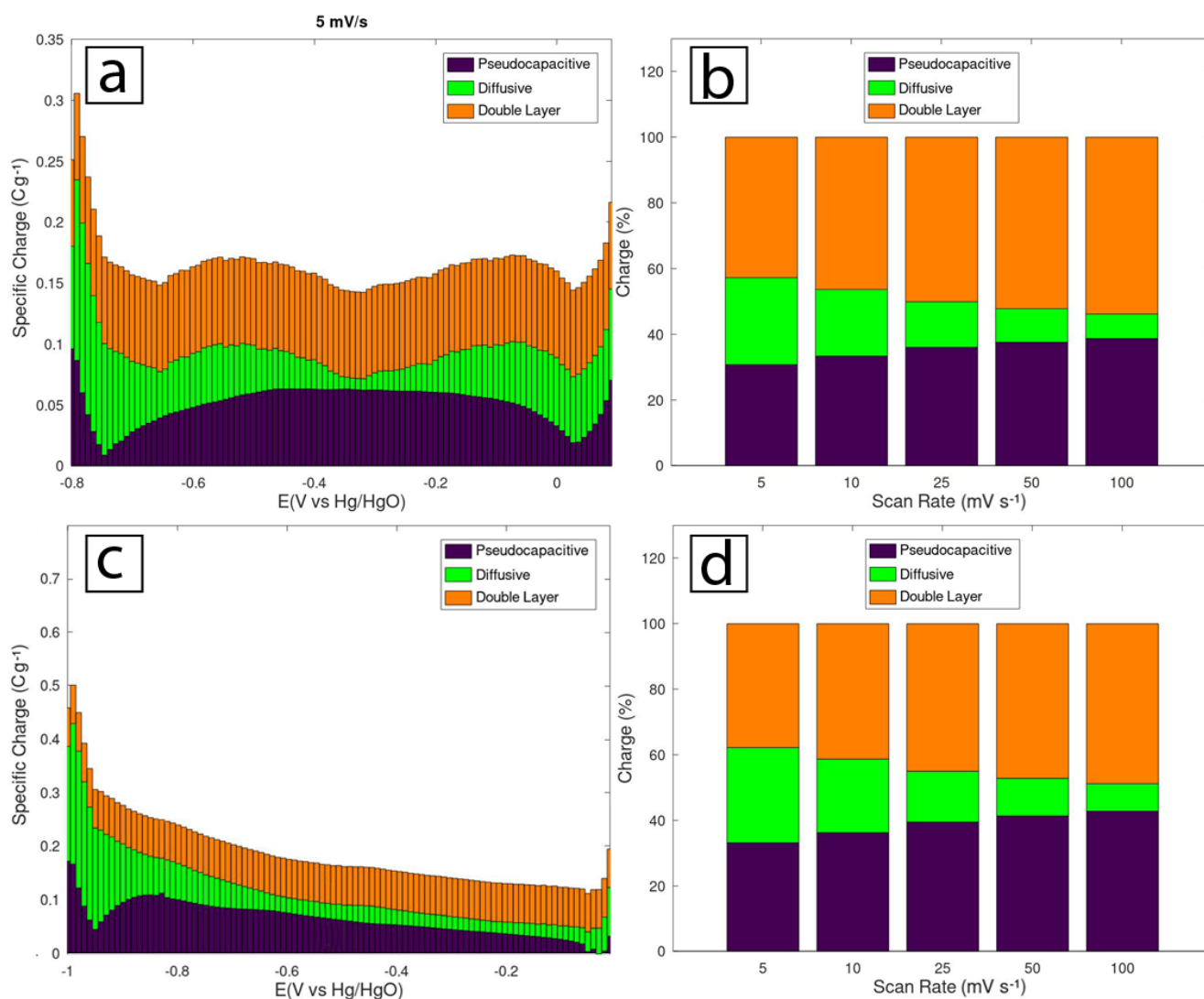


Figure 3. The specific charge of $K_{0.5}VOPO_4 \cdot 1.5H_2O$ in 3M LiOH originated by EDL, pseudocapacitive and diffusive processes at 5 mVs⁻¹ as a function of the a) applied potential and b) as a function of scan rate. The specific charge of $K_{0.5}VOPO_4 \cdot 1.5H_2O$ in 3M KOH

originated by EDL, pseudocapacitive and diffusive processes at 5 mVs^{-1} as a function of the c) applied potential and d) as a function of scan rate.

However, the stored charge from a diffusive process is lower than in the case of $\text{VOPO}_4 \cdot 2\text{H}_2\text{O}$ for the same electrolytes. This could be explained by considering the crystalline structure of these materials. In the case of $\text{VOPO}_4 \cdot 2\text{H}_2\text{O}$, the 2D tunnels are only occupied by water molecules that facilitate the ion intercalation/deintercalation process. Meanwhile in $\text{K}_{0.5}\text{VOPO}_4 \cdot 1.5\text{H}_2\text{O}$, K^+ ions and water molecules are together present in the 2D tunnels resulting in a reduction of the interlayer distance from 7.41 \AA for $\text{VOPO}_4 \cdot 2\text{H}_2\text{O}$ to 6.38 \AA . The reduction of the interlayer space is mainly due to attractive electrostatic forces caused by the presence of K^+ ions [30]. Thus, the occupied active sites by K^+ ions and the reduction of the 2D tunnels may hinder the process of ion intercalation, which in turn will decrease the amount of accumulated charge. It is reasonable to think that the smaller size of Li^+ compared to K^+ ions would allow its intercalation process to be more favorable. However, Li^+ ions intercalation should proceed via the reduction of the interlamellar space of $\text{VOPO}_4 \cdot 2\text{H}_2\text{O}$ from 7.41 \AA to 6.12 \AA [49] lower than 6.38 \AA , the interlayer distance when K^+ ions are present in the crystalline structure. Additionally, as mentioned above, the layers of vanadium and phosphorus polyhedra are displaced with respect to each other to form large cavities where K^+ cations and H_2O molecules are located. Thus, to reduce the distance between the layers to allow the intercalation of Li^+ ions, a displacement of the layers is also required together with the deintercalation of K^+ ions. Hence, the Li^+ ion intercalation requires more steps that cannot be fully carried out within the time scale used in our measurements. Subsequently, the accumulated charges decrease. In the case of 3M KOH, the low accumulated charge could be explained by the presence of the pre-existing K^+ cations in the interlayer space that cannot be intercalated/deintercalated at the scan rates (5 mVs^{-1} and above) used in this work. Additionally, in $\text{K}_{0.5}\text{VOPO}_4 \cdot 1.5\text{H}_2\text{O}$ there are CTAB molecules adsorbed at the surface, thus blocking the surface-active sites. As the scan rate increases up to 100 mVs^{-1} the main contribution to the stored charge is from the capacitive process in both electrolytes (see Figure 3b and d). This is expected, due to the high scan rate that limits the ion intercalation into the crystalline structure.

The limited ion intercalation/deintercalation process in $\text{K}_{0.5}\text{VOPO}_4 \cdot 1.5\text{H}_2\text{O}$ is related to the active thickness reached by electrolyte cations. Figure 4 shows the active thickness (see SI

for the methodology) in the applied potential during the cyclic voltammetry considering a one-electron process and a density of 2.75 g cm^{-3} . In 3M LiOH electrolyte, the active thickness is as high as 0.4 nm (0.6 unitary cells) and 0.3 nm in KOH (0.5 unitary cells). The small active thickness estimated for this electrode material in both electrolytes is caused by a low contribution of the diffusive current to the stored charge. Hence, the $\text{K}_{0.5}\text{VOPO}_4 \cdot 1.5\text{H}_2\text{O}$ particle thickness is 40 nm indicating that only 2 percent of its thickness is involved in the charge storage processes.

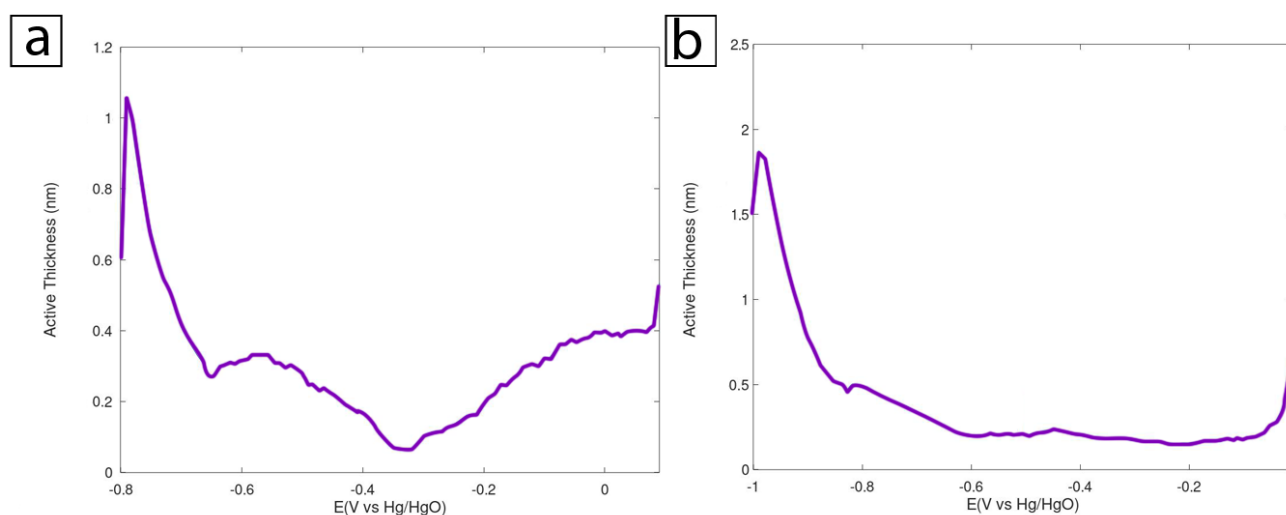


Figure 4. The active thickness of $\text{K}_{0.5}\text{VOPO}_4 \cdot 1.5\text{H}_2\text{O}$ in function of the applied potential at 5 mVs^{-1} in a) 3M LiOH, and b) 3M KOH electrolyte.

Electrochemical Impedance Spectroscopy (EIS) was performed in a frequency range of 10 mHz to 100 kHz at open circuit potential for both electrode materials $\text{VOPO}_4 \cdot \text{CTAB}$ and $\text{K}_{0.5}\text{VOPO}_4 \cdot 1.5\text{H}_2\text{O}$. Figure 5a shows the Nyquist plot of $\text{VOPO}_4 \cdot \text{CTAB}$ in both electrolytes. A large semi-circle at high frequencies indicative of large charge transfer resistance is observed in 3M LiOH. At low frequencies, the curve is parallel to the Z_{im} axis indicating a capacitive behavior in agreement with the results shown by cyclic voltammetry experiments. When 3M KOH is used, a large semi-circle is observed across the applied frequency range indicating that the charge transfer resistance is large even at low frequencies and consequently the electrode material does not show a capacitive like behavior, in agreement with the obtained cyclic voltammograms (see Figure SI4b). The Nyquist plots of $\text{K}_{0.5}\text{VOPO}_4 \cdot 1.5\text{H}_2\text{O}$ are shown in Figure 5b. In 3M LiOH, the impedance spectra show a semi-circle at high frequencies

(inset) that is associated to the electrolyte ions reaching the active surface through the components of the composite working electrode, that turns into a straight line at high/middle frequencies and a bent tail at low frequencies, indicating an ion intercalation type diffusion process [10]. This behavior is known as an open boundary finite-length Warburg diffusion [50]. However, as discussed above, the predominant charge storage process is capacitive (EDL and pseudocapacitance) and the extension of the bending tail is less predominant than in the case of $\text{VOPO}_4 \cdot 2\text{H}_2\text{O}$ in 3M LiOH [10]. In 3M KOH, the impedance spectra also show a semi-circle at high frequencies that turns into a straight line at high-middle frequencies and a bended tail at low frequencies, indicating a cation intercalation type diffusion process as in the previous case. Once again, the predominant charge storage process is capacitive, and the extension of the bending tail is low.

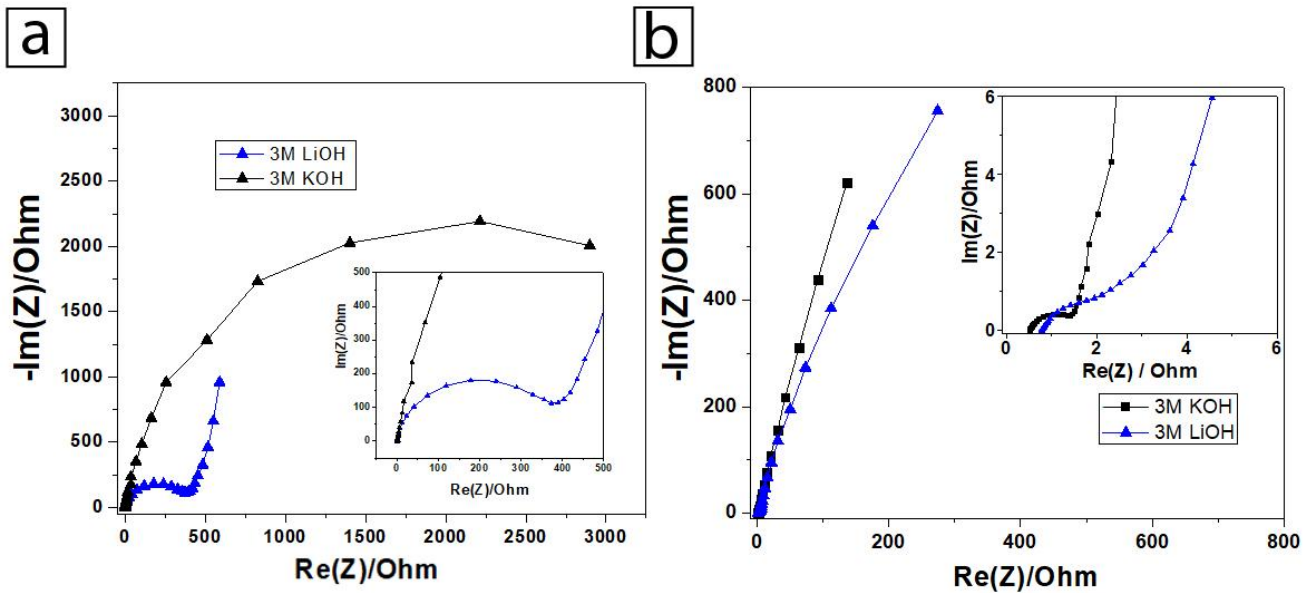


Figure 5. Electrochemical impedance spectroscopy of a) $\text{VOPO}_4 \cdot \text{CTAB}$ in 3M LiOH and 3M KOH and b) $\text{K}_{0.5}\text{VOPO}_4 \cdot 1.5\text{H}_2\text{O}$ in 3M LiOH and 3M KOH.

4. Conclusions

Two layered materials, $\text{VOPO}_4 \cdot \text{CTAB}$ and $\text{K}_{0.5}\text{VOPO}_4 \cdot 1.5\text{H}_2\text{O}$, have been synthesized to investigate the role of interlayer species on the electrochemical behavior of the related electrodes. Different molecular species in the interlayer space induce a different electrochemical behavior compared to the previous reported $\text{VOPO}_4 \cdot 2\text{H}_2\text{O}$ based electrode. Indeed, for $\text{VOPO}_4 \cdot \text{CTAB}$ electrode material the CTAB molecules block the pathway to

electrolyte ions Li^+ or K^+ . The crystalline structure of $\text{K}_{0.5}\text{VOPO}_4 \cdot 1.5\text{H}_2\text{O}$ contains K^+ ions and water molecules that hinder the intercalation/deintercalation processes. Nevertheless, according to the coupling of Trasatti and Dunn methods, the charge that arises from an intercalation process is as high as 27 and 29 % in 3M LiOH and 3M KOH, respectively. The complementary charge storage mechanisms are EDL and pseudocapacitance. Thus, three important remarks must be highlighted.

- (i) It is evidenced that the intercalation/deintercalation process is possible at the charge-discharge rates used for ECs, and it is present at least at the high scan rate of 100 mVs^{-1} as it was shown in this series of reports related to layered vanadium phosphates.
- (ii) In order to maximize the charge from an intercalation/deintercalation process, a free pathway into the 2D tunnels is necessary. A free pathway means that molecular species that avoid or hinder the ion transport must not be present in the interlayer space such as CTAB molecules. On the contrary, the presence of molecular species in the interlayer space that facilitate the ion transport like water molecules are necessary to maximize the charge from an intercalation/deintercalation process.
- (iii) The presence of ions that form part of the crystalline structure as in the case of $\text{K}_{0.5}\text{VOPO}_4 \cdot 1.5\text{H}_2\text{O}$ hinders the intercalation/deintercalation process at least at the charge rates used in the present work. The reason could be that not all the K^+ ions can be deintercalated from the crystalline structure, thus decreasing the number of accessible active sites.

Acknowledgments

This research was supported by CONACYT-Mexico, project number 255535. The authors also acknowledge the Mexican CONACYT Research Network of Energy Storage.

References

- [1]. Y. Wang, Y. Song, and Y. Xia, *Chem. Soc. Rev.*, 45, 5925 (2016).
- [2]. P. Simon and Y. Gogotsi, *Nat. Mater.*, 7, 845 (2008).
- [3]. B. Conway, *Electrochemical Supercapacitors*, Kluwer Academic, New York (1999).
- [4]. D. A. Scherson and A. Palencsár, *Electrochem Soc. Interface*, 15, 17 (2006).

- [5]. K. Wang, Q. Li, Z. Ren, C. Li, Y. Chu, Z. Wang, M. Zhang, H. Wu, Q. Zhang, *Small*, 16, 2001987 (2020).
- [6]. K. Wang, B. Lv, Z. Wang, H. Wu, J. Xu and Q. Zhang, *Dalton Trans.*, 49, 2, 411, (2020).
- [7]. K. Wang, R. Bi, M. Huang, B. Lv, H. Wang, C. Li, H. Wu, and Q. Zhang, *Inorg. Chem.*, 59, 10, 6808 (2020).
- [8]. Y. Guo, K. Wang, Y. Hong, H. Wu and Q. Zhang, *Dalton Trans.* (2021).
- [9]. J. Zuñiga, R. Lucio Porto, I. Moreno, T. Brousse, J. Aguilar Martínez and L. López Pavón, *J. Electrochem. Soc.*, 165, 10, A2349 (2018).
- [10]. J. Zúñiga, S. González, E. Le Calvez, R. Lucio Porto, I. Moreno, T. Brousse, L. López Pavón, *J. Electrochem. Soc.* 168, 070531 (2021).
- [11]. L. Athouel, F. Moser, R. Dugas, O. Crosnier, D. Bélanger, T. Brousse. *ECS Trans.* 16, 119 (2008).
- [12]. Chen, Dandan and Li, Jiangfeng and Wu, Qingsheng, *J. Nanopart. Res.*, 21 (2019)
- [13]. P. Chomkhuntod, N. Ma, S. Kosasang, S. Duangdangchote, N. Phattharasupakun, C. Jangsan, and M. Sawangphruk, *ACS Appl. Energy Mater.*, 3, 2, 1402 (2020).
- [14]. P. Xiong, R. Ma, N. Sakai, X. Bai, S. Li, and T. Sasaki, *ACS Appl. Mater. Interfaces*, 9,7, 6282 (2017).
- [15]. D. Chen, D. Ding, X. Li, G. Waller, X. Xiong, M. A. El-Sayed, and M. Liu, *Chem. Mater.*, 27, 19, 6608 (2015).
- [16]. J. M. Li, K. H. Chang, and C. C. Hu, *Electrochem. commun.*, 12, 12, 1800 (2010).
- [17]. H. Yin, C. Song, Y. Wang, S. Li, M. Zeng, Z. Zhang, Z. Zhu, and K. Yu., *Electrochim. Acta*, 111, 762 (2013).
- [18]. Z. Tong, H. Xu, G. Liu, J. Zhao, and Y. Li, *Electrochem. commun.*, 69, 46 (2016).
- [19]. A. Byeon, M. Boota, M. Beidaghi, K.V. Aken, J.W. Lee, Y. Gogotsi, *Electrochem. Commun.*, 60, 199 (2015).
- [20]. L. Kong, C. Zhang, J. Wang, D. Long, W. Qiao, L. Ling, *Mater. Chem. Phys.*, 149–150, 495 (2015).
- [21]. J. Zhang, H. Chen, X. Sun, X. Kang, Y. Zhang, C. Xu, and Y. Zhang, *J. Electrochem. Soc.*, 164, A820 (2017).
- [22]. L. Kong, C. Zhang, J. Wang, W. Qiao, L. Ling, D. Long, *Sci. Rep.*, 6, 21177 (2016).
- [23]. X. Li, J. Shao, J. Li, L. Zhang, Q. Qu, H. Zheng, *J. Power Sources*, 237, 80 (2013).
- [24]. Y. Liu, S.P. Jiang, Z. Shao, *Mater. Today Adv.*, 7, 100072 (2020).
- [25]. J. B. Mitchell, W. C. Lo, A. Genc, J. Lebeau, and V. Augustyn, *Chem. Mater.*, 29, 9, 3928 (2017).

- [26]. H. Jiang, Y. Zhang, Z. Pan, L. Xu, J. Zheng, Z. Gao, T. Hu, C. Meng and J. Wang, *Mater. Chem. Front.*, 4, 1434 (2020).
- [27]. X. Shan, F. Guo, D. S. Charles, Z. Lebens-Higgins, S. A. Razek, J. Wu, W. Xu, W. Yang, K. L. Page, J. C. Neufeind, M. Feygenson, L. F. J. Piper and X. Teng, *Nat. Commun.*, 4975 (2019).
- [28]. N. Park, Kwand Kim, and Soon Ho Chang, *Electrochem. Commun.*, 3, 10, 553 (2001).
- [29]. C. Wu, X. Lu, L. Peng, K. Xu, X. Peng, J. Huang, G. Yu, and Y. Xie, *Nat. Commun.*, 4, 1 (2013).
- [30]. S. L. Wang, H. Y. Kang, C. Y. Cheng, and K.H. Lii, *Inorg. Chem.*, 30, 3496 (1991).
- [31]. R. B. Viana, A.B.F. da Silva and A. S. Pimentel. *Adv. Phys. Chem.*, 1, (2012).
- [32]. X. Yu, L. Zhao, X. Gao, X. Zhang, and N. Wu., *J. Solid State Chem.*, 179, 1525 (2006).
- [33]. J. Zhu, H. He, L. Zhu, X. Wen, and F. Deng., *J. Colloid Interface Sci.*, 286, 239 (2005).
- [34]. R. A. Vaia, R. K. Teukolsky and E. P. Giannelis. *Chem. Mater.* 6, 1017 (1994).
- [35]. X. Yu, *Micropor. Mesopor. Mat.*, 98, 70 (2007).
- [36]. N.V. Venkataraman, S. Vasudevan. *J. Phys. Chem.* 105, 1805 (2001).
- [37]. Z. Jiang, J. Xie, D. Jiang, X. Wei, M. Chen., *Cryst. Eng. Comm.*, 15, 560 (2013).
- [38]. A. Datta, S. Sakthivel, M. Kaur, A. M. Venezia, G. Pantaleo, and A. Longo, *Micropor. Mesopor. Mat.*, 128, 213 (2010).
- [39]. S. Dasgupta, M. Agarwal, and A. Datta., *J. Mol. Catal. A: Chem.*, 223, 167 (2004).
- [40]. P. Borah and A. Datta, *Appl. Catal. A-Gen.*, 376, 1, 19 (2010).
- [41]. N. Chen, J. Zhou, Q. Kang, H. Ji, G. Zhu, Y. Zhang, S. Chen, J. Chen, X. Feng, and W. Hou, *J. Power Sources*, 344, 185 (2017).
- [42]. S. J. Lim, J. T. Vaughey, W. T. A. Harrison, L. L. Dussack, A. J. Jacobson, and J. W. Johnson, *Solid State Ion.*, 84, 3, 219 (1996).
- [43]. B. M. Azmi, T. Ishihara, H. Nishiguchi, and Y. Takita, *Electrochim. Acta*, 48, 2, 165 (2002).
- [44]. H. R. Tietze, *Aust. J. Chem.*, 34, 10, 2035 (1981).
- [45]. S. Trasatti, *J. Electroanal. Chem.*, 123, 121 (1981).

- [46]. Y. Zhang, Y. Zhang, H. Feng, X. Wu, L. Wang, A. Zhang, T. Xia, H. Dong, X. Li, and L. Zhang, *Int. J. Hydrogen Energ.*, 34, 4889 (2009).
- [47]. S. Ardizzone, G. Fregonara and S. Trasatti, *Electrochim. Acta*, 35 , 263, (1990).
- [48]. T. Brezesinski, J. Wang, J. Polleux, B. Dunn and S. H. Tolbert, *J. Am. Chem. Soc.* 131, 1802 (2009).
- [49]. J. Hyung, J. W. Heo, M. S. Chae, and S. Hong, *ChemSusChem.*, 12, 1069 (2019).
- [50]. V. S. Muralidharan, *Anti-Corros. Method. M.*, 44, 1, 26, (1997).